Structure of two-, four-, and six-quasiparticle isomers in ^{174}Yb and *K*-forbidden decays

G. D. Dracoulis,[1] G. J. Lane,[1] F. G. Kondev,[2] A. P. Byrne,[1,3] T. Kibédi,[1] H. Watanabe,[1] I. Ahmad,[4] M. P. Carpenter,[4] S. J. Freeman,[4] R. V. F. Janssens,[4] N. J. Hammond,[4] T. Lauritsen,[4] C. J. Lister,[4] G. Mukherjee,[4,5] D. Seweryniak,[4] P. Chowdhury,[5] and S. K. Tandel[5]

[1]*Department of Nuclear Physics, Research School of Physical Sciences and Engineering, Australian National University, Canberra, A.C.T. Australia 0200*

[2]*Nuclear Engineering Division, Argonne National Laboratory, Argonne, Illinois 60439*

[3]*Department of Physics, The Faculties, Australian National University, Canberra, A.C.T. Australia 0200*

[4]*Physics Division, Argonne National Laboratory, Argonne, Illinois 60439*

[5]*Department of Physics, University of Massachusetts Lowell, Lowell, Massachusetts 01854*

(Received 27 December 2004; published 29 April 2005)

The stable nucleus ^{174}Yb has been studied using deep-inelastic reactions and time-correlated γ-ray spectroscopy. New intrinsic states assigned include a 370-ns isomer at 1765 keV, which we associate with a predicted $K^\pi = 7^-$ two-quasineutron configuration. Analysis of the alignment and in-band properties of its rotational band, identified using time-correlated coincidences, allows characterization of the configuration. The properties of a newly identified rotational band built on the known 830-μs isomer at 1518 keV support the 6^+, 2-quasineutron configuration assignment proposed previously. The 6^+ band is fed by a four-quasiparticle, $K^\pi = 14^+$ isomer at 3699 keV and several higher multiquasiparticle states, including a six-quasiparticle isomer at 6147 keV with $K = (22,23)$. The results are discussed in terms of the states predicted on the basis of multiquasiparticle calculations. The anomalously fast *K*-forbidden transition strengths from the 14^+ isomer are attributed to either *K* mixing in the neutron configuration or to random mixing in the high-level-density region. The 7^- isomer decays are not abnormal, whereas the very hindered E2 transition from the 6^+ isomer to the ground-state band remains unexplained.

DOI: 10.1103/PhysRevC.71.044326 PACS number(s): 21.10.Re, 21.10.Tg, 23.20.Lv, 27.70.+q

I. INTRODUCTION

As is common with stable deformed nuclei in the rare-earth region, spectroscopic information on high-spin states in the $N = 104$ isotope ^{174}Yb is limited, because it is accessible neither via fusion-evaporation reactions with stable beams nor via incomplete-fusion reactions. Coulomb excitation and inelastic scattering provide the main information on the structure of the ground-state rotational band [1], which is known to about spin $20\hbar$. A feature of the level scheme is the presence of a 830-μs meanlife isomer at 1518 keV, populated in (d,p) and other relatively low-spin reactions, including neutron capture on ^{173}Yb and β decay from ^{174}Tm and ^{174}Lu [1–3]. Although commonly associated with the $K^\pi = 6^+$ state from the two-quasineutron (ν^2) Nilsson configuration $5/2^-[512] \otimes 7/2^-[514]$ [2], the spin-parity assignment recorded in the data compilations [1] has been the subject of considerable conjecture. Identification of the rotational band based on this isomer would be an important component of its proper characterization. Further, it is an important state in terms of defining pairing strengths and residual interactions that, together with the Nilsson-orbital energies, control the excitation energies of the intrinsic states. Multiquasiparticle calculations, such as those carried out in Ref. [4], suggest that the 7^- state from the $7/2^+[633] \otimes 7/2^-[514]$ ν^2 configuration may be at a comparable energy to the 6^+ level. Experimentally, the equivalent 6^+ and 7^- states are only 50 keV apart in ^{180}Os [5] and 70 keV apart in the isotone ^{178}W. In the latter case, the 6^+ state is at least partly depressed by mixing with a two-proton configuration that will not occur at low energy in ^{174}Yb. To further complicate matters, the 8^- state from the related $9/2^+[624] \otimes 7/2^-[514]$ two-quasineutron configuration drops rapidly in energy in this region, as the neutron Fermi level passes through midshell for the $i_{13/2}$ orbitals. This occurs sufficiently quickly to result in the 1050 keV, 11.5 s 8^- isomer in ^{176}Yb and, equivalently, higher up in the proton shell, to the 1.1 ms 8^- isomer in ^{182}Os.

A comparable level of uncertainty arises in the odd-proton neighbor ^{175}Lu where a 1391-keV isomer with a similar lifetime is known [6–8]. It has been assumed to have $K^\pi = 19/2^+$ obtained by coupling of the $7/2^+[404]$ proton to the 6^+ core. As in ^{174}Yb, restrictions on multipolarities on the basis of conversion coefficients [6] and hindrances, become ambiguous because of the relatively high energy of the transitions and the long lifetimes. Taken together these admit alternative combinations of mixed, high multipolarities. The ^{175}Lu assignment is consistent with multiquasiparticle calculations, but these rely in part on constraining parameters from the core states in ^{174}Yb.

Here, we report new results on the spectroscopy of intrinsic states and rotational bands in ^{174}Yb, obtained from (so-called) deep-inelastic reactions, with time correlated γ-ray techniques. The results include a number of new isomeric states for which configuration assignments are suggested. Other results on high-*K* isomers in ^{177}Lu and ^{179}Ta from the same series of measurements have recently been published [9,10].

II. EXPERIMENTAL PROCEDURES

The main experiments used 6.0 MeV/nucleon, ^{136}Xe beams provided by the ATLAS facility at Argonne National

Laboratory. Nanosecond pulses, separated by about 1 μs, were incident on targets of natural Lu (97% ^{175}Lu, 2.6% ^{176}Lu), Lu enriched to 47% in ^{176}Lu (with which the majority of data were collected), and ^{174}Yb enriched to ~95%. The targets were approximately 6-mg/cm^2-thick metallic foils with 25-mg/cm^2 Au foils at the rear. The beam conditions (~20% above the Coulomb barrier) result in inelastic processes with single and multiple transfer of nucleons as well as inelastic excitation of the target and projectile nuclei [11–13].

Gamma rays were detected in Gammasphere [14] with 100 Compton-suppressed detectors in operation. About 2×10^8, 2×10^9, and 2×10^8 coincidence events of threefold and higher were collected for the ^{175}Lu, ^{176}Lu, and ^{174}Yb targets, respectively.

Complementary measurements aimed at clarifying details of the level scheme were obtained using the ^{173}Yb(^{18}O,^{17}O)^{174}Yb reaction with the CAESAR array and pulsed beams provided by the ANU 14UD Pelletron facility. These reactions populate states up to relatively low spins (~8$\hbar$), but they provided useful independent information on lifetimes and assignments.

III. ANALYSIS TECHNIQUES

The nonselective nature of the reaction process means that a broad range of nuclei and nuclear states is excited, leading to very complicated data sets. However, recent developments in software [15] allowed the efficient production of appropriate coincidence matrices with different time and gating γ-ray conditions. With the resulting flexibility, a variety of time conditions relating both the time difference between specific γ rays, and their time relative to the beam pulses, could be exploited. Decays from isomers were isolated by selecting events occurring between beam pulses and a large number of known isomers in the Yb, Lu, Hf, and Ta nuclei were observed. Comparison of the yields seen with the different targets, together with the observation of characteristic X rays in coincidence, formed the initial basis for assignment of new structures, some of which cannot be directly assigned to a specific isotope because of the very long lifetimes of the isomers that intervene. In the ^{174}Yb case, for example, the relative yield is about a factor of three larger with the ^{174}Yb target, than with either of the Lu targets, reflecting the larger cross section for inelastic excitation compared to proton transfer (and additional neutron) transfer.

The primary sources of information for the present work were therefore as follows:

1. γ–γ–γ coincidence cubes with a broad prompt (±140 ns) relative time condition and an absolute time condition defining whether the γ rays were observed in-beam or between beam pulses. These were constructed for the data sets from each of the three targets for yield comparisons and to provide independent information on possible contaminants.
2. γ–γ–γ cubes with a prompt (±140 ns) relative time condition, but with absolute time conditions selecting six contiguous time regions, about 110 ns wide, covering the out-of-beam period, for the higher statistics (^{176}Lu) data set. These were particularly valuable for isolating short-lived isomers, and removing long-lived contaminants and, with appropriate gating, for measuring lifetimes.
3. Two-dimensional γ–γ matrices constructed with specific γ-ray gates (single and double) and specific relative and absolute time conditions, chosen to isolate structures above and below isomeric states, with minimal contamination. These will be referred to in detail in the subsequent discussions.

Particular care was taken to gain-match the detectors in energy and to match the times (measured with time-to-digital converters) for each detector, taking account of both linear and nonlinear differences that can be significant in the Gammasphere electronics.

For convenience, in the subsequent presentation and discussion, transition and level energies are quoted to the nearest kilo-electron-volt, except in instances of possible ambiguity.

A. γ–γ angular correlations

The techniques for extraction of γ–γ correlations for symmetric multiple detector arrays have been outlined in Ref. [16] in the general case when the reaction process produces spin alignment, as in fusion, evaporation reactions. The alignment to be expected in the present reactions that involve a variety of process and conditions (energy and particle transfer, etc.), leading to any particular product is not well defined but is likely to be minimal in most cases. Transitions below long-lived isomeric states should also be deoriented. Analysis of the angular distributions of various products in the present measurements shows no evidence for significant alignment. Under these circumstances it is reasonable to assume no alignment, at least as a first approximation, in which case a simplified formulation is valid.

There are a large number of angular combinations between the detectors of Gammasphere but these can be grouped into approximately eight average angular differences with $\Delta\Theta = 0^\circ, 20^\circ, 35^\circ, 41^\circ, 53^\circ, 61^\circ, 71^\circ,$ and 85°. There are fewer combinations for the 0° point in the present experimental configuration, hence in most cases its statistics were too low to be reliable. The other angles have between 400 and 1000 combinations, allowing a correlation analysis to be carried out for transitions of relatively low absolute strength. The analysis requires extensive evaluation of the relative efficiencies using internal normalizations to account for differences in deadtime effects and so on.

Angular correlation coefficients (A_{kk}) were obtained from the fit of the γ–$\gamma(\Delta\Theta)$–coincidence intensities obtained from spectra generated with gates on pairs of transitions, to the following equation:

$$W(\Theta) = 1 + A_{22} P_2(\cos\Delta\Theta) + A_{44} P_4(\cos\Delta\Theta). \quad (1)$$

In some cases, it is possible to sum sequences of stretched quadrupole gates, for example, to obtain higher statistics. The experimental A_{22} coefficients of γ_1–γ_2 cascades can be related to the orientation parameters (B_k) of the first transition and the directional distribution coefficients (A_k) of the second

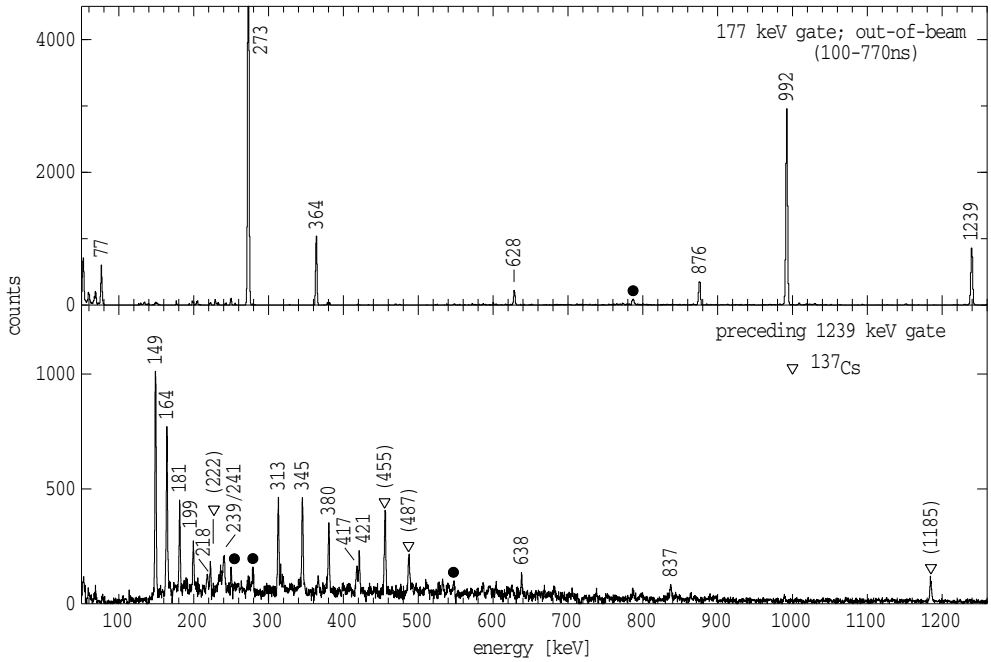

FIG. 1. Coincidence γ-ray spectra for ^{174}Yb. (Upper panel) Gate on the 177 keV, $4^+ \rightarrow 2^+$ transition in the period between beam pulses, as indicated. (Lower panel) Transitions preceding the delayed 1239 keV γ ray. Contaminants are indicated by filled circles.

transition as follows [17]:

$$A_{kk} = B_k(\gamma_1)A_k(\gamma_2), \tag{2}$$

where

$$B_k(\gamma_1) = \frac{F_k(L_1L_1I_0I_1) - 2\delta(\gamma_1)F_k(L_1L_1'I_0I_1) + \delta^2(\gamma_1)F_k(L_1'L_1'I_0I_1)}{1+\delta^2(\gamma_1)} \tag{3}$$

and

$$A_k(\gamma_2) = \frac{F_k(L_2L_2I_2I_1) + 2\delta(\gamma_2)F_k(L_2L_2'I_2I_1) + \delta^2(\gamma_2)F_k(L_2'L_2'I_2I_1)}{1+\delta^2(\gamma_2)}. \tag{4}$$

L_1 and L_2 are the lowest multipole orders of the first and second transition, $L_1' = L_1 + 1$, $L_2' = L_2 + 1$. I_0, I_1, and I_2 are the respective spins of the first, intermediate, and lowest levels involved in the cascade. Values of F_k are given in the tabulation of Hamilton [18]. Least-squares fits to the present results were carried out using the prescription of Ref. [19].

IV. RESULTS AND LEVEL SCHEME

Figure 1 shows the spectrum of γ-rays in coincidence with the 177 keV, $4^+ \rightarrow 2^+$ transition in the out-of-beam region (from 100 ns on). The 992 keV γ ray is the transition from the known 6^+ isomer at 1518 keV, but the 876 and 1239 keV γ rays are assigned to the decay of a new isomeric state at 1765 keV. The lifetime of 370(16) ns obtained for this state from the gated intensities with respect to the beam pulsing in the deep-inelastic measurement, and confirmed in the complementary study with the (^{18}O,^{17}O) reaction, is ideal for isolating transitions feeding that isomer. The spectrum of γ rays feeding the 1239-keV transition (lower panel of Fig. 1) from the measurement with the target enriched in ^{176}Lu (but that contains over 50% ^{175}Lu) shows mainly the $\Delta I = 1$ and $\Delta I = 2$ members of the rotational band placed on top of the isomer and transitions assigned to the excitation of one of the complementary products, ^{137}Cs (one-proton transfer from ^{175}Lu to ^{136}Xe). Two of these transitions (455 and 487 keV) coincide approximately with where crossover transitions within the rotational band are expected. Population via transfer of a proton and a neutron from ^{176}Lu should also lead to excitations in ^{138}Cs, but the level scheme of that nucleus is poorly known, and it is likely to have isomeric states that would complicate its observation. (Note that the probability for population of excited states in the complementary partners will generally decrease as the excitation energy and angular momentum of the product of interest increases. In the case of high excitation, there can also be neutron emission before γ-decay [11,12].)

The level scheme deduced for ^{174}Yb is given in Fig. 2. As well as the 876-keV and 1239-keV branches, a 247-keV transition is observed in delayed coincidence with the band members above the 1765-keV isomer, but it does not feed the ground-state band. It is placed as a connection between the 7^- and 6^+ isomers. A weak branch from the 1765-keV isomer is also observed to the (5^-) member of the known $K^\pi = 2^-$ octupole band, further confirming the placement. Analysis of the decay branching and implied transition strengths from the

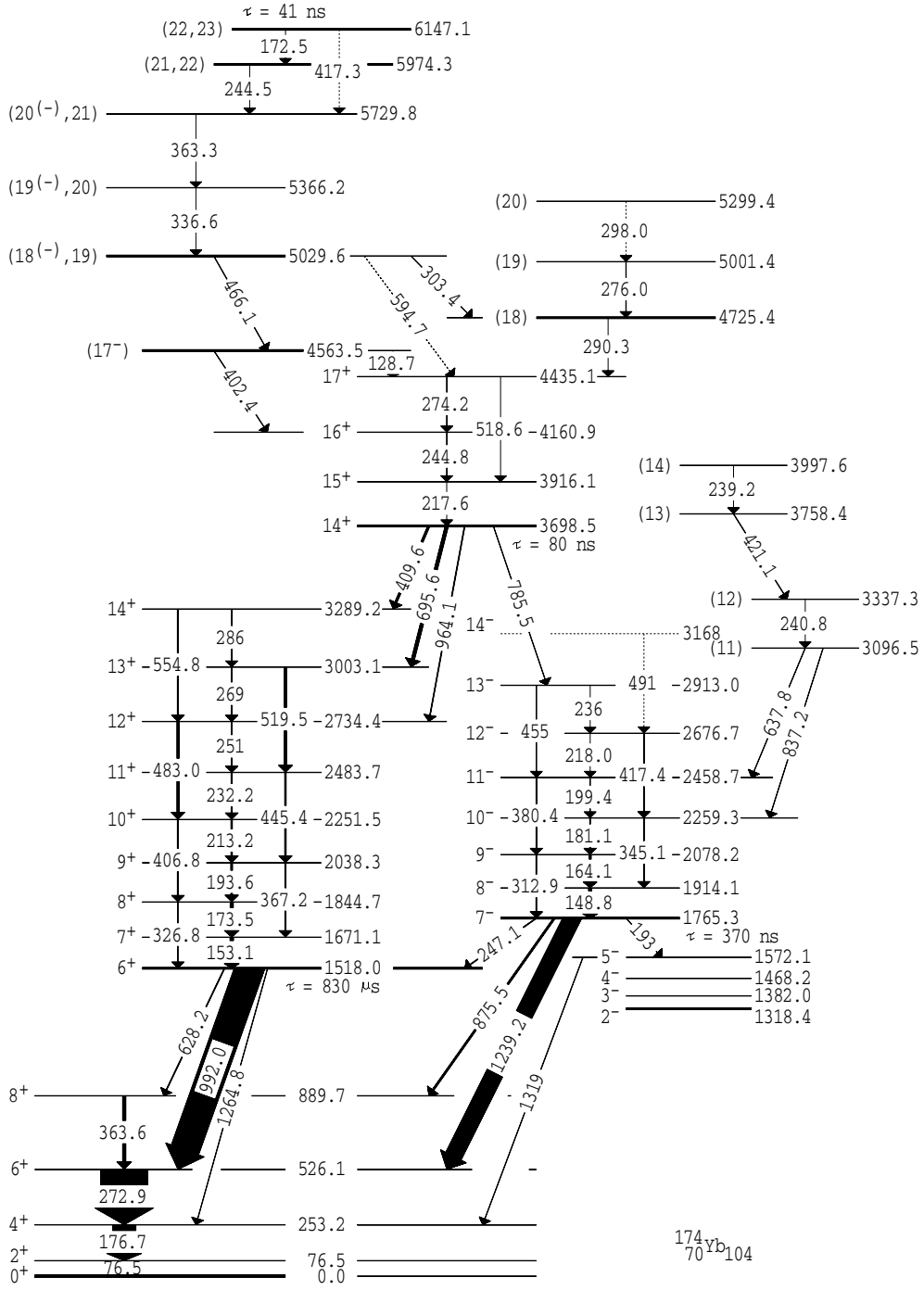

FIG. 2. Levels of ^{174}Yb observed in the present study. Note that the transitions known to deexcite the lower members of the 2^- octupole band are not shown.

relatively short lifetime (to be discussed later), the absence of a direct branch to the 4^+ ground-state band member and the correlation results, all support a firm $K^\pi = 7^-$ assignment. Except for the low-intensity 786-keV branch from the 14^+ isomer at 3699 keV, population of the 7^- band is essentially prompt. Side-feeding into the 10^- and 11^- states from several levels that are possible intrinsic states and fragments of their rotational bands is seen, as shown in Fig. 2.

The lifetime curve for the main branch from the 7^- isomer obtained in the ^{173}Yb(^{18}O,^{17}O)^{174}Yb reaction with a chopped beam (macroscopic pulses of 100 ns separated by 4 μs) is presented in Fig. 3. In these measurements, the 1239-keV transition is only partially resolved from a 1242-keV transition that depopulates the 2^- state of the octupole band that is also populated in β decay from ^{174}Lu formed in the proton-transfer channel, giving a residual long-lived component.

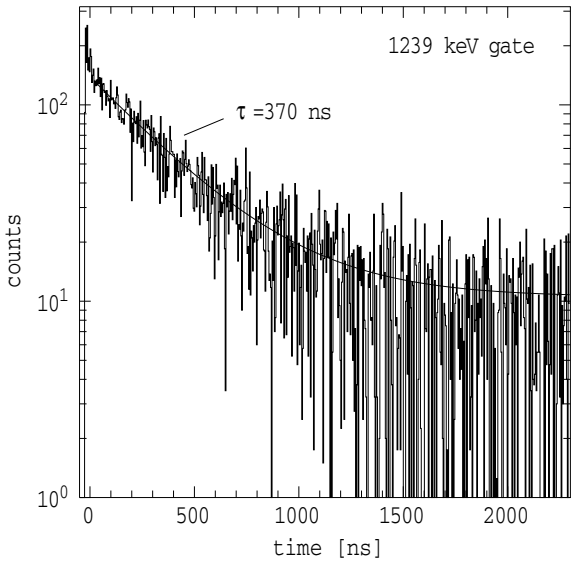

FIG. 3. Time spectrum and associated fit for the 1239-keV transition obtained in the ^{18}O-induced measurements.

The lifetime of the 6^+ isomer is too long to allow correlations between transitions above and below it, but the $7^+ \rightarrow 6^+$ in-band cascade transition at 153 keV was known from neutron capture and β decay [1]. Double-gating on candidate transitions, together with the 153-keV transition, resulted in observation of the band structure. The band is fed from a relatively short-lived isomer with connecting transitions at 410, 696, and 964 keV. These, and the rotational band extending to spin 14^+, are evident in the spectrum of Fig. 4. This spectrum was constructed by summing double gates on the band members, as observed in a γ–γ–γ cube confined to a relatively short time region (30–100 ns) after the beam pulse. The weak transitions at 218, 245, and 274 keV, and so on, are placed above the isomer at 3699 keV (see Fig. 2), but they are also fed by yet another high-lying isomer, with a short lifetime. Hence, their appearance in the delayed coincidence spectrum of Fig. 4.

On the basis of the angular correlations, the γ-ray branching ratios and the related decay strengths, to be discussed further below, the spin and parity of the 3699-keV state is assigned as 14^+. Note that the K change between this state and the $K = 6$ band is large, hence the relatively short lifetime leads to severe constraints on the possible spin and K changes. (Note also that the E1 branch of 786 keV to the 13^- member of the 7^- band confirms again the placement of these structures in ^{174}Yb.)

Figure 5 is a sum of coincidence gates on the main transitions placed above the 14^+ isomer, as obtained from a matrix constructed with the same double γ-ray energy gates and time constraints as used to produce Fig. 4, with the additional condition that the selected γ rays *preceded* in time the decay of the 14^+ isomer.

Some caution is needed in interpreting these results quantitatively, because the narrow time gates that are required can produce distortions in the apparent intensities. The 274-keV line, for example, lies at the peak of the Gammasphere efficiency and lower energy lines may be reduced in intensity because of the inferior intrinsic timing response of large volume Ge detectors and the time cuts. Construction of the scheme above was also complicated by the presence of the 172.5-keV line, which is close in energy to the strong 173.5-keV line in the 6^+ band below, whereas the 193-keV peak in Fig. 5 is attributed to feed-through of the strong 193-keV line in the 6^+ band, although the presence of an additional, (unplaced) 193-keV line in the upper part of the scheme cannot be completely ruled out.

The lifetime of the 14^+ isomer at 3699 keV was obtained by projecting the intermediate time differences with gates on transitions above and below the isomer. The time spectrum is shown in the lowest panel of Fig. 6, with a fit resulting in a meanlife of 80(6) ns. Note that in this case, because of

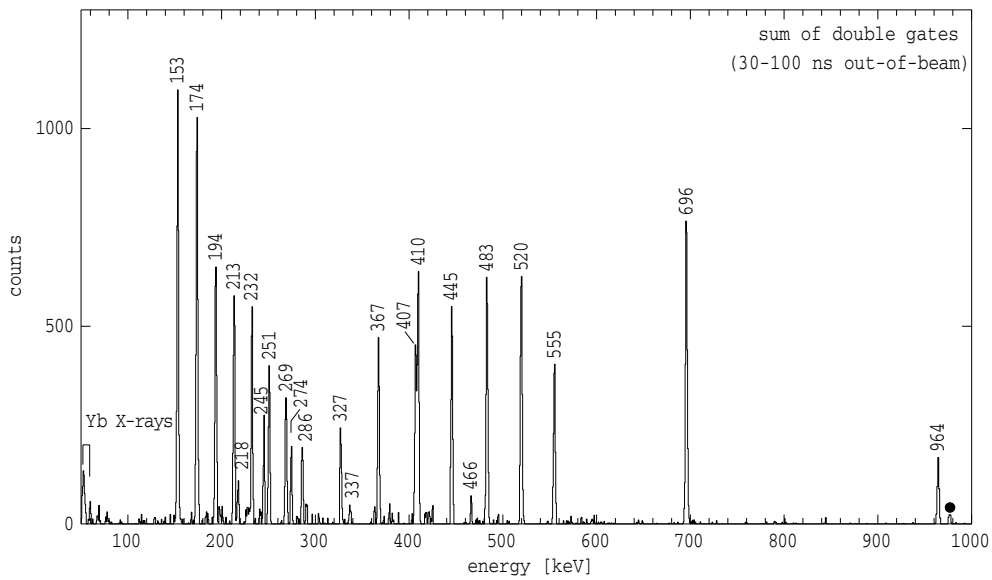

FIG. 4. Spectrum constructed from a combination of double γ-ray gates on transitions assigned to the $K^\pi = 6^+$ band, constrained to the 30- to 100-ns region after the beam pulse.

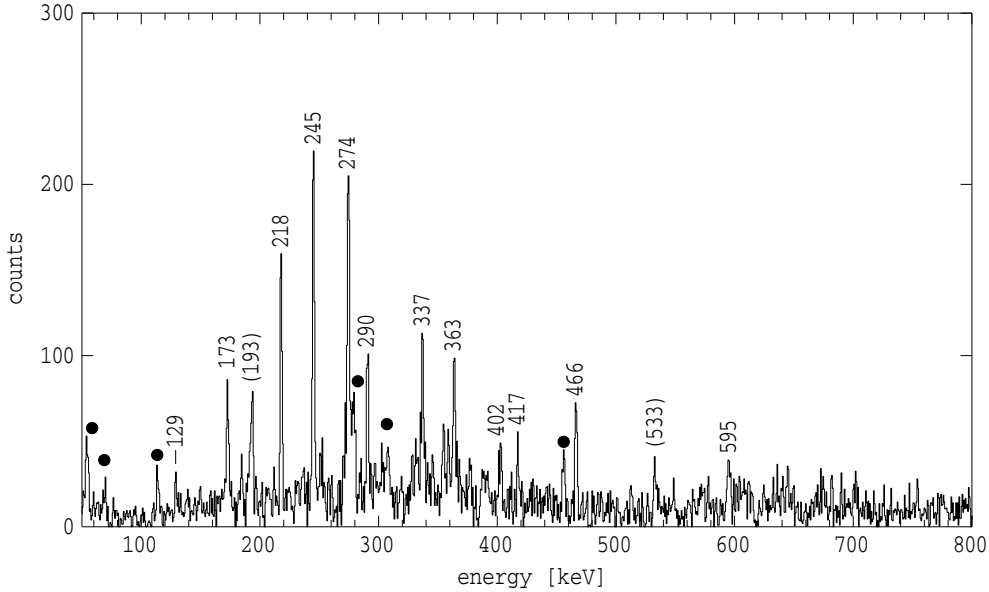

FIG. 5. Spectrum constructed from a combination of γ-ray gates on transitions observed to precede the $K^{\pi} = 14^{+}$ isomer. Contaminants are indicated by filled circles.

the complex gating conditions, the time region within about 30 ns of time-zero is distorted and therefore was not included in the fit.

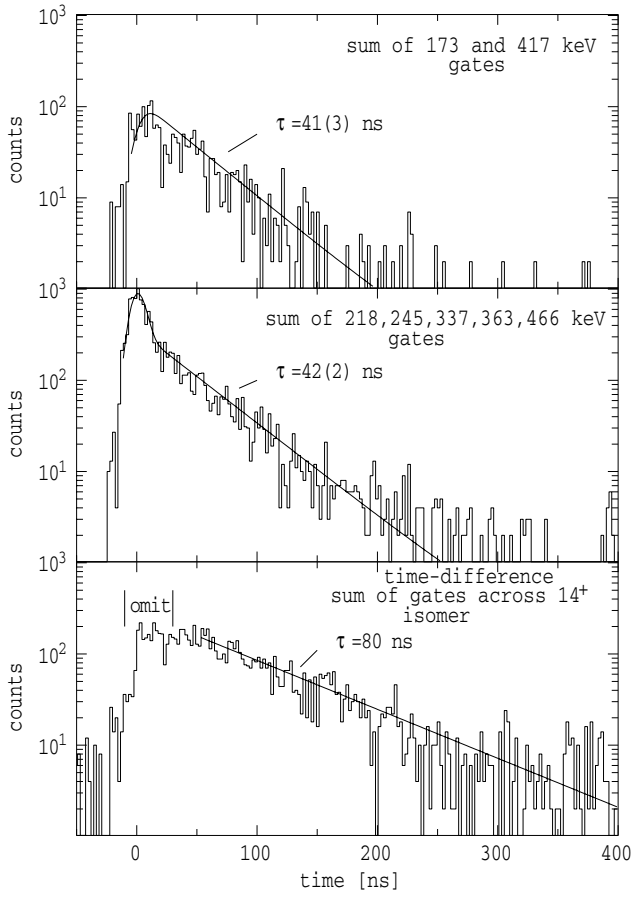

FIG. 6. Time spectra and fits illustrating the short isomers.

The two upper panels of Fig. 6 present time spectra for combinations of the main transitions above the 14^{+} isomer. This was constructed from a two-dimensional matrix with γ rays above the 14^{+} isomer (selected from delayed double gating as described previously) on one axis and the absolute time with respect to the beam pulse on the other. The delayed component in these spectra is from a $\tau = 41(2)$ ns isomer (meanlife adopted from a number of fits) at the top of the scheme, as indicated in Fig. 2. Note that the 417-keV transition is placed as directly deexciting the isomer, but the order of the 173- and 245-keV transitions could not be established unambiguously, and the transitions could be in the reverse order. The time spectrum for the 173-keV transition would be consistent with this possibility but a definitive time spectrum for the 245-keV transition could not be obtained because of the presence of the other 245-keV transition in the cascade.

The 218-, 245-, and 274-keV transitions are suggested to be members of the rotational band based on the 14^{+} isomer. This conjecture and some aspects of the scheme in this region remain somewhat uncertain, partly because of the low intensity and also because not all crossover transitions within the 14^{+} band have been observed. (At higher K values, E2 crossover transitions become increasingly less competitive with the M1 cascades.) The 519-keV transition connecting the 17^{+} and 15^{+} states coincides in energy with the strong 519-keV transition in the 6^{+} band. Similarly, the 245-keV transition placed as directly deexciting the uppermost isomer, coincides in energy with the 245-keV, $16^{+} \rightarrow 15^{+}$ transition, which therefore, exhibits strong self-coincidences. Some levels assigned as band members could be, instead, intrinsic states. That qualification aside, the multiple branches from the 5030-keV state suggest that it is an intrinsic state with rotational band members located above it. The 6147-keV, 41-ns isomer must be an intrinsic state, and it is likely that the 5974-keV level to which it decays is

TABLE I. Angular correlations for decays from isomers in ^{174}Yb.

Initial state J^π	$E(\gamma_2)$ (keV)	Transition	$E(\gamma_1)$ (keV)	Assignment	A_{22}	A_{44}	$\delta(\gamma_1)$
	520	$13^+ \to 11^+$	696	$14^+ \to 13^+$	−0.186(27)	−0.009(38)	−0.20(5)
	269	$13^+ \to 12^+$	696	$14^+ \to 13^+$	+0.344(59)	+0.135(76)	
14^+	555	$14^+ \to 12^+$	410	$14^+ \to 14^+$	+0.173(36)	+0.064(47)	-0.30^{+53}_{-32}
	286	$14^+ \to 13^+$	410	$14^+ \to 14^+$	−0.279(74)	−0.090(104)	
	483	$12^+ \to 10^+$	964	$14^+ \to 12^+$	+0.233(72)	−0.026(95)	
7^-	273 177	$6^+ \to 4^+$ $4^+ \to 2^+$	1239	$7^- \to 6^+$	−0.062(8)	+0.003(11)	+0.02(1)
7^-	364 273 177	$8^+ \to 6^+$ $6^+ \to 4^+$ $4^+ \to 2^+$	876	$7^- \to 8^+$	−0.101(6)	−0.006(9)	0.00(1)
6^+	273 177	$6^+ \to 4^+$ $4^+ \to 2^+$	992	$6^+ \to 6^+$	+0.030(5)	+0.078(7)	-1.80^{+6}_{-7}

also an intrinsic state. Although their properties are not well defined, the states at 4725-keV (which decays by a 290-keV transition) and the 4563-keV state are presumably of the same character.

Unfortunately, there is no evidence of measurable intermediate lifetimes (with upper limits of approximately $\leqslant$5 ns), which would help with the identification of intrinsic states and with the ordering of the transitions referred to above. The absence of lifetimes, however, does imply transitions between states of similar K values. This is considered further below.

A. Angular correlations

The statistics in the present experiment were sufficient to obtain angular correlation results for the stronger transitions from the 1518- and 1765-keV isomeric states and for the three transitions from the 3699-keV isomer. In the latter case, the data selected were confined to the 30- to 100-ns delayed region to reduce contaminants. The results are summarized in Table I and Fig. 7. Similarly, correlations were obtained for a number of the dipole cascade transitions within the $K^\pi = 6^+$ band, allowing mixing ratios to be deduced, as shown in Table II.

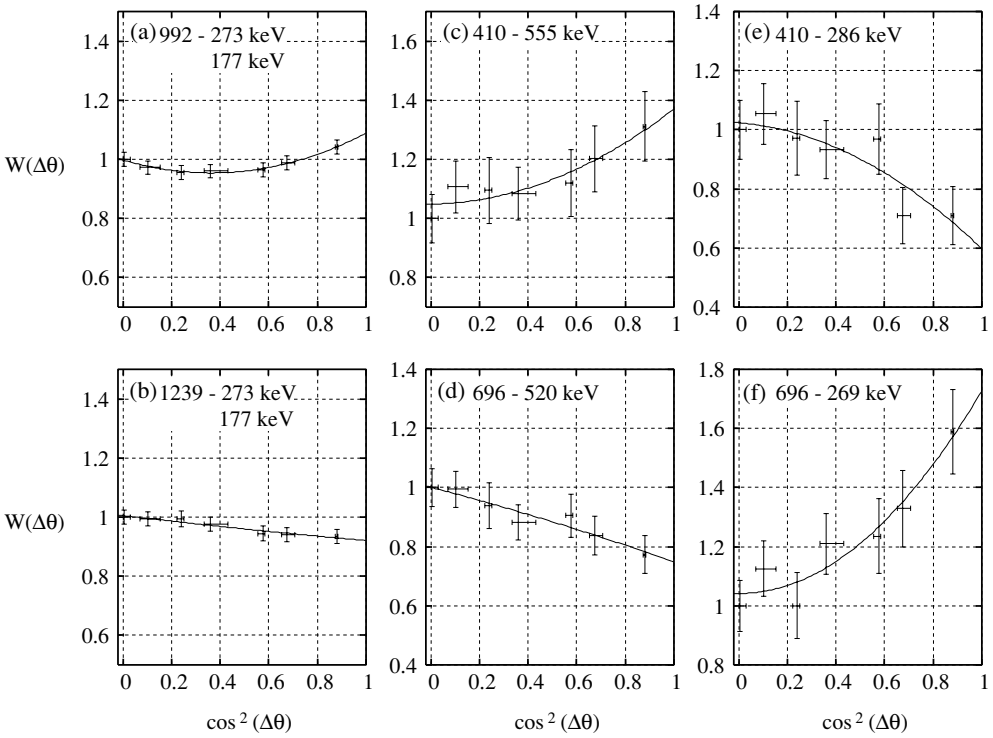

FIG. 7. Angular correlations for selected transitions in ^{174}Yb.

TABLE II. Angular correlations and mixing ratios for transitions within the $K^\pi = 6^+$ band.

$E(\gamma_1)$ (keV)		$E(\gamma_2)$ (keV)		A_{22}	A_{44}	$\delta(\gamma_2)$	$g_K - g_R$[a]
520	$13^+ \rightarrow 11^+$	232	$11^+ \rightarrow 10^+$	−0.278(39)	−0.071(54)	-1.48^{+103}_{-53}	-0.101^{+27}_{-229}
483	$12^+ \rightarrow 10^+$	213	$10^+ \rightarrow 9^+$	−0.253(41)	−0.115(58)	-1.77^{+146}_{-103}	-0.085^{+31}_{-401}
445	$11^+ \rightarrow 9^+$	194	$9^+ \rightarrow 8^+$	−0.377(76)	−0.109(107)	-0.93^{+47}_{-85}	-0.163^{+78}_{-167}
407	$10^+ \rightarrow 8^+$	174	$8^+ \rightarrow 7^+$	−0.257(101)	−0.007(140)	-1.07^{+79}_{-138}	-0.144^{+81}_{-411}
367	$9^+ \rightarrow 7^+$	153	$7^+ \rightarrow 6^+$	−0.276(66)	+0.063(92)	-0.63^{+30}_{-135}	-0.246^{+168}_{-229}

[a]Taking $Q_0 = 7.51$.

V. LEVEL SCHEME, ASSIGNMENTS, AND CONFIGURATIONS

A. Transition strengths and band properties

The transition strengths in Table III are given in terms of the hindrance factor $F = \tau/\tau_W$, the ratio of the partial mean-lives to the Weisskopf estimates τ_W, and the reduced hindrances $f_\nu = F^{1/\nu}$, where the degree of forbiddenness for multipolarity λ is given by the shortfall between the required K change and the transition multipolarity, $\nu = \Delta K - \lambda$.

B. Two-quasiparticle isomers

1. 6^+ isomer at 1518 keV ($\tau = 830$ μs)

The earlier spin and parity assignment to this state was based initially on the conversion coefficient of the 992-keV transition that suggested a mixed M1/E2 multipolarity [2]. This multipolarity, however, cannot be distinguished from the E1/M2 possibility on the basis of the conversion coefficient alone. A γ–γ correlation between the 992-keV transition and the 273-keV $6^+ \rightarrow 4^+$ transition was claimed [20] to establish a 6^+ assignment for the 1518-keV state, but in later measurements it was pointed out by Schmidt, Michelich, and Funk [21] that the angular correlation was also compatible with a $7^- \rightarrow 6^+ \rightarrow 4^+$ sequence if E1/M2/E3 multipolarity mixing were considered. They obtained values of E1(68 ± 7%) + M2(5 ± 2%) + E3(27 ± 7%) for that solution, a combination which also reproduces the conversion coefficient. Nevertheless, they also conceded that a definitive assignment was not possible on the basis of the spectroscopic information but argued that the 6^+ assignment was favored because the alternative 7^- assignment implied several E3 transition strengths that, although retarded, were relatively fast compared to expected values. Angular distributions were also obtained for the 992-keV transition from $(n, n'\gamma)$ studies [22] that were stated to be consistent with the γ–γ correlations, but that could equally well be interpreted as being from a mixed $7^- \rightarrow 6^+$ transition. Krane *et al.* [23] claimed an unambiguous 6^+ assignment, but this was on the basis of a combination of their low-temperature orientation results, together with the correlation results of Schmidt *et al.* [21].

Although we cannot add new spectroscopic information on the decay transitions from the present results except to

TABLE III. Transition strengths and hindrances for decays from isomers in ^{174}Yb.

Initial state I^π	E_γ (keV)	I_γ relative	$M\lambda$	α_T	$B(E\lambda)$ (e^2 fm$^{2\lambda}$)	Hindrance	ν	f_ν[a]
6^+	628	2.0(2)	E2	0.010	$2.00(22)\times10^{-8}$	$2.88(32)\times10^{8}$	4	130
830(50) μs	992	96.2(12)	M1/E2	0.030	$6.73(42)\times10^{-11}$	$2.66(17)\times10^{10}$	5	122
	1265	1.8(6)	E2	0.0024	$5.4(20)\times10^{-9}$	$1.07(40)\times10^{10}$	4	322
7^-	247	4.8(2)	E1	0.047	$5.40(42)\times10^{-9}$	$3.72(29)\times10^{8}$	0	
370(16) ns	876	13.4(12)	E1	0.0019	$3.37(36)\times10^{-10}$	$5.97(64)\times10^{9}$	6	43; *13.5*
	1239	81.5(39)	E1	0.0010	$7.25(56)\times10^{-10}$	$2.78(21)\times10^{9}$	6	38; *11.8*
	193	0.35(12)	E2	0.305	$2.9(9)\times10^{-2}$	$1.99(62)\times10^{3}$	4	12.6
14^+	410	32.3(22)	M1	0.071	$3.22(34)\times10^{-6}$	$5.54(58)\times10^{5}$	7	6.6
80(6) ns	696	52.4(21)	M1	0.0183	$1.07(10)\times10^{-6}$	$1.68(16)\times10^{6}$	7	7.7
	964	13.9(9)	E2	0.004	$1.65(17)\times10^{-3}$	$3.50(36)\times10^{4}$	6	5.7
	786	1.4(3)	E1	0.0024	$2.18(44)\times10^{-10}$	$9.2(18)\times10^{9}$	6	45.8; *14.4*
(14^-)	410	32.3(22)	E1	0.0096	$3.66(39)\times10^{-8}$	$5.49(59)\times10^{7}$	7	12.8; *4.8*
80(6) ns	696	52.4(21)	E1	0.0030	$1.21(11)\times10^{-9}$	$1.66(15)\times10^{8}$	7	14.9; *5.5*
	964	13.9(9)	M2	0.020	$1.52(16)\times10^{-2}$	$3.36(35)\times10^{2}$	6	2.6
	786	1.4(3)	M1	0.014	$2.02(40)\times10^{-8}$	$8.9(17)\times10^{7}$	6	21.1

[a]Values in italics include an additional factor of 10^3 in the expected single-particle hindrance for E1 transitions.

confirm the mixed multipolarity of the 992-keV transition (see Table I), indirect confirmation of the 6^+ assignment comes from the properties of the band established above the isomer. The angular correlation obtained for the 992-keV transition and presented later is essentially identical to that obtained in the early decay work [20], consistent with the assumption of no alignment. Observation of the 7^- intrinsic state, which was not known previously, effectively removes any question of ambiguity. Linking of both the 6^+ and 7^- structures through the 14^+ isomer further supports the spin assignments.

2. 7^- state at 1765 keV ($\tau = 370$ ns)

This isomer mainly decays to the 6^+ and 8^+ levels of the ground-state band and to the 6^+ isomer, with a weak, low-energy branch of 193 keV to the 5^- member of the 2^- octupole band. Consideration of the branching ratios and transition strengths leaves only 7^- or 7^+ as plausible possibilities. The angular correlations (Fig. 7 and Table I) are consistent with nearly pure stretched dipole character for both the 876- and 1239-keV transitions to the 8^+ and 6^+ states of the ground-state band. The alternative 7^+ assignment for the 1765-keV state is effectively excluded because it would imply the presence of an M2 branch to the 5^- state with a hindrance of about 5. This would be abnormally fast for an M2 transition, even in the absence of K hindrance. As indicated in Table III, with the 7^- assignment, both E1 decays have f_ν values of about 40, which is acceptable, although E1 transitions are usually hindered by additional factors of about 10^3. Inclusion of that factor leads to effective f_ν factors (indicated in italics in Table III) that are smaller by a factor of 3. Also, the E2 branch to the 5^- state of the octupole band has a low reduced hindrance of about 12. Both facts can be qualitatively understood in terms of Coriolis mixing, because the presence of the $7/2^+[633]$, $i_{13/2}$ orbital in the 7^- state (see later for the configuration assignment) will introduce significant K mixing. A calculation for the equivalent state in the isotone ^{180}Os gave 5% $K = 5$, 17% $K = 6$, and 81% $K = 7$ (Ref. [5]) and similar admixtures would be expected here. In addition, octupole bands have significant Coriolis matrix elements between the $K = 0, 1, 2$, and 3 projections of the 3^- octupole vibration [24] so that both initial and final states will have mixed K values.

C. Four- and six-quasiparticle isomers

1. 14^+ state at 3699 keV ($\tau = 80$ ns)

The 3699-keV isomer has a relatively short lifetime and decays predominantly to the 12^+, 13^+, and 14^+ levels of the 6^+ band, with a weak branch to the 13^- state of the 7^- band. The spin/parity possibilities are limited to 13^-, $14^\pm$, or 15^-. The E1 transitions in the case of the 13^- possibility have forbiddenness $\nu = 6$ and implied reduced hindrances of $f_\nu \sim 25$, without adjustment for the additional hindrance expected for E1 transitions. That make this possibility unlikely, as does the absence of branches to the 11^- and 12^- states of the 7^- band that would be energetically favored. The 15^- possibility also implies E1, M2, and E3 strengths to the 6^+ band, which are unlikely. Similarly the 14^- option, shown for comparison in Table III, gives unacceptably low hindrances for the implied E1 and M2 transitions. This leaves 14^+ as the only alternative, albeit still one with unusually enhanced strengths. These are discussed in a later section.

Independent of these considerations, the angular correlations presented in Fig. 7 and Table I lead to a firm spin 14 assignment with characteristic $I \rightarrow I$, $I \rightarrow I - 1$, and $I \rightarrow I - 2$ correlations for the 410-, 696-, and 964-keV transitions, respectively.

2. $K = (22,23)$ state at 6147 keV ($\tau = 41$ ns) and other intrinsic states

As can be seen from Fig. 5 the absolute intensity available after the coincidence gating required to isolate transitions above the 14^+ isomer is low, hampering a quantitative analysis. Nevertheless, on the basis of intensity balances, the 129-keV transition from the 4564-keV state has a total conversion coefficient $\alpha_T \leqslant 0.3$. This value is consistent only with E1 multipolarity and therefore spin/parity of 17^- or 18^- for the 4564-keV state; however, there is a residual uncertainty in the data analysis, hence the parity is given in parentheses in the level scheme. The 18^- possibility implies M2 multipolarity for the 402-keV transition to the 16^+ band member, which is unlikely in the absence of any significant lifetime. The 5030-keV state probably has $I^\pi = 18^-$ or, less likely, spin 19. Both possibilities are shown on the level scheme, but the 19^+ alternative is problematic because of the 595-keV transition (it would also have to be M2, although it is tentative), whereas the 19^- alternative would require the 466-keV γ ray to be of M2 character.

The 337- and 363-keV transitions are assumed to form the dipole cascade within the rotational band based on the 5030-keV state, whereas the feeding from the isomer at 6147-keV and the state at 5974-keV (which would be at 5902-keV if the order of the 173- and 245-keV transitions were reversed) is consistent with assignment of spin 21 and 22 for the 5974 and 6147 intrinsic states, or somewhat less likely, spins 22 and 23, respectively.

The 4725-keV state probably has spin 18, with the fragmented decay of the 5030-keV level being explained in terms of the K-selection rule that favors transitions to other high-K states rather than to the $K = 14^+$ band.

D. In-band branching ratios and alignments; configuration assignments

1. $g_K - g_R$ values

Standard rotational model formulae allow the extraction of the quantity $|g_K - g_R|/Q_0$, which is characteristic of the Nilsson configurations involved, from the measured $\Delta I = 2/\Delta I = 1$ intensities. That ratio λ is given by the following:

$$\lambda = \frac{(I+1)(I+K-1)(I-K-1)}{2K^2(2I-1)} \frac{E_\gamma^5(I \rightarrow I-2)}{E_\gamma^5(I \rightarrow I-1)} \frac{\delta^2}{1+\delta^2},$$

TABLE IV. Values of g_K and $g_K - g_R$ for proposed configurations.

K^π	Configuration		g_K[a]	$g_K - g_R$[b]	$\lvert g_K - g_R \rvert$
	ν	π	predicted		Measured[c]
6^+	$5/2^-[512]7/2^-[514]$		$+0.06 + \textit{0.02}$	$-0.29 - \textit{0.33}$	0.437(6)
7^-	$7/2^+[633]7/2^-[514]$		$+0.10 + \textit{0.07}$	$-0.25 - \textit{0.28}$	0.261(7)
14^+	$5/2^-[514]7/2^-[514]\otimes$ $7/2^+[633]9/2^+[624]$		$-0.15 - \textit{0.08}$	$-0.50 - \textit{0.43}$	
	or				
	$5/2^-[512]7/2^-[514]$	$7/2^-[523]9/2^-[514]$	$+0.75 + \textit{0.75}$	$+0.40 + \textit{0.40}$	

[a]Nilsson values or semiempirical values (in italics).
[b]Taking $g_R = 0.35$.
[c]Weighted averages of values in Table V.

where E_γ is in mega-electron-volts and the mixing ratio δ is as follows:

$$\delta = 0.933 \frac{E_\gamma(I \to I-1)}{\delta\sqrt{I^2-1}} \frac{Q_0}{g_K - g_R}.$$

For multiquasiparticle configurations,

$$g_K = \frac{1}{K} \sum_i \Omega_i g_{\Omega_i}.$$

Large $g_K - g_R$ values will favor the M1 cascade transitions over the E2 crossover transitions, as will high-K values. Values of g_Ω can be estimated from Nilsson wave functions for specific orbitals and they can also be extracted from experiment for well-defined bands in nearby nuclei. A selection of these is shown in Table IV for the configurations of importance here.

The measured value of the quadrupole moment for the 2^+ state of ^{174}Yb is 7.7(9) eb but a recent accurate measurement for the $7/2^-[514]$ state in ^{175}Yb corresponds to $Q_0 = 7.51(13)$ eb [25]; hence, because these nuclei should have very similar deformations, the latter value has been used in extracting the experimental $g_K - g_R$ values. These are listed in Table V for the 6^+, 7^-, and 14^+ bands.

The branching ratios for the 6^+ band give a weighted mean of $|g_K - g_R| = 0.437(6)$ (not including the uncertainty in Q_0), which is higher than the expected value given in Table IV. The value of $|g_K - g_R| = 0.261(7)$ obtained for the 7^- band from the branching ratios (Table V is in good agreement with the predicted value). Because the $7/2^-[514]$ orbital is common to both (as is g_R), there is only limited opportunity for adjustment of these values although Coriolis mixing is significant in the $7/2^+[633]$ orbital and this puts additional (systematic) uncertainty on its theoretical value and on the extracted value.

Also, the angular correlation results for the in-band dipole transitions for the 6^+ band given in Table II all give negative mixing ratios, which implies a negative value for $g_K - g_R$ because Q_0 is positive, but the magnitudes are lower than expected and at face value, not all consistent with the magnitude obtained from the branching ratios. However, the errors in the mixing ratios are both large and asymmetric because of the complex shape of the χ^2 minima in these cases, and there may be systematic errors present because of the assumption that there is no alignment in the reaction. This is certainly a valid assumption for transitions below long-lived isomers (as in the case of transitions below the 6^+ isomer) but it might be more problematic for short-lived states. (See Ref. [26] for comments on spin alignment in such reactions.)

2. Alignments

Another feature characteristic of the orbital configuration is the angular momentum alignment that reflects the Coriolis mixing specific to each orbital [27]. The net alignment is approximately additive, but with some nonlinear effects caused largely by pairing reduction because of blocking (see, for example, Ref. [28]).

Figure 8 presents the net alignments obtained with a common reference, chosen to produce an approximately flat curve for the ground-state band (labeled gsb). Several features are apparent. The 6^+ band shows a relatively small alignment,

TABLE V. Branching ratios and $(g_K - g_R)$ values for states of the proposed 6^+ and 7^- bands in ^{174}Yb.

J^π	$E_\gamma(\Delta I = 1)$ (keV)	$E_\gamma(\Delta I = 2)$ (keV)	λ	$\lvert g_K - g_R \rvert$ exp.
$K^\pi = 6^+$				
14^+	286	555	2.36(23)	0.475^{+27}_{-23}
13^+	269	520	2.31(15)	0.431^{+17}_{-15}
12^+	251	483	1.91(12)	0.422^{+16}_{-14}
11^+	232	445	1.31(7)	0.448^{+14}_{-13}
10^+	213	407	0.85(7)	0.471^{+23}_{-21}
9^+	193	367	0.69(4)	0.407^{+12}_{-11}
8^+	174	327	0.24(2)	0.479^{+20}_{-18}
$K^\pi = 7^-$				
12^-	218	417	1.84(35)	0.278^{+37}_{-28}
11^-	199	380	1.59(17)	0.247^{+18}_{-15}
10^-	181	345	0.85(7)	0.273^{+13}_{-12}
9^-	164	313	0.46(3)	0.256^{+10}_{-9}
$K^\pi = 14^+$				
17^+	274	519	$\leqslant 0.09$	$\geqslant 0.53$

[a]Taking $Q_0 = 7.5$ eb.

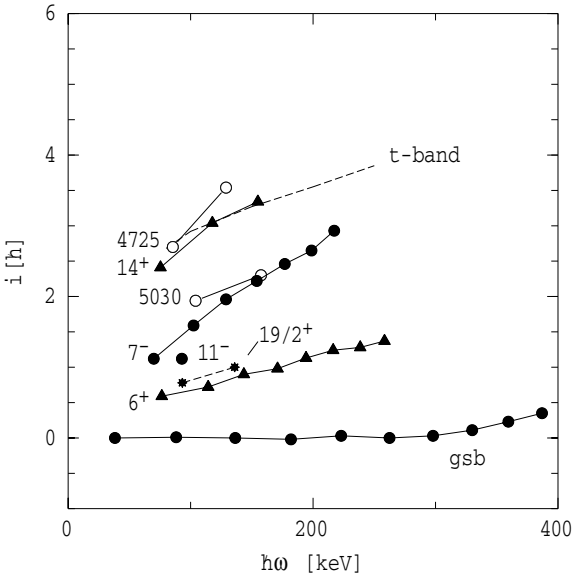

FIG. 8. Comparison of alignments of the bands in ^{174}Yb and (i) the alignment estimated for the *t*-band configuration obtained by combining the $i_{13/2}$ orbitals in the odd neutron neighbors and (ii) the $K^\pi = 19/2^+$ band in ^{175}Lu [8]. All alignments have been extracted using a common reference with parameters $\Im_0 = 39$ MeV$^{-1}\hbar^2$ and $\Im_1 = 70$ MeV$^{-3}\hbar^4$.

consistent with the proposed ν^2 configuration that does not contain orbitals strongly affected by Coriolis mixing. It is very similar to the alignment of the fragment of the $K^\pi = 19/2^+$ band in ^{175}Lu [8], which, as discussed, should be closely related. In contrast, the proposed 7^- band has significantly more alignment, as expected for a configuration involving the $7/2^+[633]$ neutron orbital, clearly supporting the proposed configuration. Of the two possibilities for the 14^+ band, only the ν^4 $5/2^-[512]7/2^-[514]7/2^+[633]9/2^+[624]$ configuration, the so-called *t*-band [29–31] for the 6^+ configuration, would have significant alignment. The relatively large alignment observed compares well with an empirical estimate (dashed curve labeled *t*-band in Fig. 8) obtained by summing the average of the signature-split alignments observed for the $7/2^+[633]$ band in ^{173}Yb [32] and the alignment of the $9/2^+[624]$ band now identified (from the present series of experiments [33]) in ^{175}Yb. This clearly supports the ν^4 configuration given later.

The same argument can be made for configuration assignments to the bands beginning at 5030-keV (possible 18^- assignment) and the band at 4725 keV (assignment of (18)). The band structure in this region of the scheme is uncertain, but at face value, the alignment suggests that the lower state, at 4725 keV, has a configuration related to the 14^+ isomer, whereas the 5030-keV state does not.

VI. MULTIQUASIPARTICLE CALCULATIONS

Calculation of the expected multiquasiparticle spectrum was carried out using an approach similar to that of Jain *et al*. [34], but with some modification, as outlined in recent publications (for example, ref [35]). The procedure involves a choice of single-particle levels and the neutron and proton pairing strengths G_ν and G_π and, to avoid the limitations that cause collapse of the BCS solutions in regions of low and nonuniform level densities, the use of the Lipkin-Nogami formulation for calculation of the pairing correlation.

The calculations use the prescription given by Nazarewicz *et al*. [36] to treat the Fermi level and pairing gaps self-consistently, to include particle-number conservation, and to have blocked states removed for multiquasiparticle configurations. For these calculations a space of three oscillator shells was used for each of the neutron and proton spaces, giving 64 levels (128 states) with 30 active protons and 64 active neutrons.

The Nilsson orbitals were calculated assuming constant deformations of $\epsilon_2 = 0.266$ and $\epsilon_4 = 0.048$ [27] to give the initial set of single-particle states. (These deformations differ somewhat from those predicted by Ref. [37] that give $\epsilon_2 = 0.258$ and $\epsilon_4 = 0.073$.) Subsequently, the single-particle energies for the neutron levels close to the Fermi surface used in the calculations were adjusted to reproduce approximately the average of the observed one-quasineutron states in the odd-neutron neighbors ^{173}Yb and ^{175}Yb, whereas the odd-proton orbitals were adjusted by considering the ^{173}Tm and ^{175}Lu one-quasiproton levels. Note that the one-quasiparticle states are calculated using the same self-consistent procedures as is used in the multiquasiparticle cases. As discussed in the comparisons below, the proton orbitals move rapidly in this region and empirical information on the proton orbitals in ^{173}Tm is scarce, with only the $1/2^+[411]$, $7/2^-[523]$ and $3/2^+[411]$ orbitals well established, and a candidate for the $9/2^-[514]$ intrinsic state known. The $7/2^+[404]$ orbital, which is the ground state in ^{175}Lu, is not known.

The pairing strengths were taken as $G_\nu = 18.0/\mathrm{A}$ and $G_\pi = 20.8/\mathrm{A}$, the same values selected in evaluations of a range of Ta and Lu isotopes [4,8,9,35,38]. (Note that we have not corrected the one-quasiparticle energies for the rotational contribution to the band-head energy, which is of the order of $\frac{\hbar^2}{2\Im}K$, nor has this been added to the predicted energies.)

The two-, four-, and six-quasiparticle states predicted to be lowest are listed in Tables VI and VII. The residual interactions that play a role in determining the lowest states are also given in the tables. These are calculated using the generalized form given by Jain *et al*. [34] for summing the two-quasiparticle contributions for each combination using the observed Gallagher-Moszkowski energies. The values listed differ slightly in some cases from those that would follow from the compilation of π-π, ν-ν, and π-ν interactions in Ref. [34] because of a reevaluation by Kondev [39] of some of the empirical values.

In the multiquasiparticle case, the residual interaction is the linear sum of attractive and repulsive components. When medium to high-Ω orbitals are involved, only the states with maximum $K = \sum_i \Omega_i$ are usually of interest. Reversal of say, one orbital projection Ω_j, will result in a state with $K = K_{\max} - 2 \times \Omega_j$, and even if that state is favored in energy over the $K_{\max.}$ state, it will usually be non-yrast and less likely to be populated. However, the situation can be different when

TABLE VI. Positive parity two-, four-, and six-quasiparticle states in ^{174}Yb from multiquasiparticle calculations.

K^{π} [a]	Configuration[b]		E_{qp}	$E_{\rm res}$	$E_{\rm calc}$	$E_{\rm expt}$
	ν	π		(keV)		
6^+	$5/2^-7/2^-$		1506	−128	1378	1518
8^+	$7/2^+9/2^+$		2023	+200	2223	
8^+		$7/2^-9/2^-$	2496	+200	2696	
12^+	$1/2^-7/2^+7/2^-9/2^+$		3465	−173	3292	
12^+	$7/2^+7/2^-$	$1/2^+9/2^-$	3911	−155	3756	
12^+	$5/2^-9/2^+$	$1/2^+9/2^-$	3951	+165	4116	
13^+	$7/2^-9/2^+$	$1/2^+9/2^-$	4193	−155	4038	
14^+	$5/2^-7/2^+7/2^-9/2^+$		3355	+263	3618	3699
14^+	$5/2^-7/2^-$	$7/2^-9/2^-$	4001	−79	3922	
15^+	$7/2^-9/2^+$	$7/2^-7/2^+$	4748	−400	4348	
16^+	$7/2^+9/2^+$	$7/2^-9/2^-$	4519	+143	4662	
17^{+*}	$5/2^-7/2^+7/2^-9/2^+$	$1/2^+7/2^+$	5734	−77	5657	
18^+	$5/2^-7/2^+7/2^-9/2^+$	$1/2^+7/2^+$	5734	+715	6449	
18^+	$1/2^-5/2^-7/2^-9/2^+$	$7/2^-7/2^+$	5929	−523	5406	
19^+	$5/2^+7/2^+7/2^-9/2^+$	$1/2^+9/2^-$	6335	+256	6591	
20^+	$1/2^-7/2^+7/2^-9/2^+$	$7/2^-9/2^-$	5961	+23	5984	
22^+	$5/2^-7/2^+7/2^-9/2^+$	$7/2^-9/2^-$	5851	+55	5906	6147

[a]An asterisk indicates nonmaximal couplings.

[b]Configurations as follows:

(ν): $1/2^-$:$1/2^-[521]$; $9/2^+$:$9/2^+[624]$; $5/2^-$:$5/2^-[512]$; $7/2^-$:$7/2^-[514]$; $7/2^+$:$7/2^+[633]$; $5/2^+$:$5/2^+[642]$.

(π): $7/2^-$:$7/2^-[523]$; $9/2^-$:$9/2^-[514]$; $7/2^+$:$7/2^+[404]$; $5/2^+$:$5/2^+[402]$; $1/2^+$:$1/2^+[411]$; $3/2^+$:$3/2^+[411]$.

TABLE VII. Negative-parity two-, four-, and six-quasiparticle states in ^{174}Yb from multiquasiparticle calculations.

K^{π} [a]	Configuration[b]		E_{qp}	$E_{\rm res}$	$E_{\rm calc}$	$E_{\rm expt}$
	ν	π		(keV)		
7^-	$7/2^+7/2^-$		1753	−93	1660	1765
7^-	$5/2^-9/2^+$		1794	+184	1978	
8^-	$7/2^-9/2^+$		2036	−93	1943	
11^-	$1/2^-5/2^-7/2^-9/2^+$		3218	−160	3058	(3097)
11^-	$5/2^-7/2^-$	$1/2^+9/2^-$	3662	−156	3506	
13^-	$5/2^-7/2^-$	$7/2^-7/2^+$	4216	−531	3685	(3758)
13^-	$7/2^+9/2^+$	$1/2^+9/2^-$	4180	+147	4327	
14^-	$5/2^+7/2^+7/2^-9/2^+$		4178	+321	4199	
15^-	$7/2^+7/2^-$	$7/2^-9/2^-$	4250	+84	4334	
15^-	$5/2^-9/2^+$	$7/2^-9/2^-$	4290	−1	4289	
16^-	$7/2^-9/2^+$	$7/2^-9/2^-$	4532	+58	4590	
17^-	$1/2^-7/2^+7/2^-9/2^+$	$1/2^+9/2^-$	5621	−255	5366	
18^{-*}	$5/2^-7/2^+7/2^-9/2^+$	$1/2^+9/2^-$	5512	−60	5452	(5030)
19^-	$5/2^-7/2^+7/2^-9/2^+$	$1/2^+9/2^-$	5512	+233	5745	
19^-	$1/2^-5/2^-7/2^-9/2^+$	$7/2^-9/2^-$	5715	−92	5623	
19^-	$1/2^-7/2^+7/2^-9/2^+$	$7/2^-7/2^+$	6176	−415	5761	
20^-	$5/2^-7/2^+7/2^-9/2^+$	$3/2^+9/2^-$	6309	+114	6423	
20^-	$5/2^-7/2^+7/2^-9/2^+$	$7/2^-5/2^+$	6419	+56	6365	
21^-	$5/2^-7/2^+7/2^-9/2^+$	$7/2^-7/2^+$	6066	+128	5930	5974

[a]An asterisk indicates nonmaximal couplings.

[b]Configurations as follows:

(ν): $1/2^-$:$1/2^-[521]$; $9/2^+$:$9/2^+[624]$; $5/2^-$:$5/2^-[512]$; $7/2^-$:$7/2^-[514]$; $7/2^+$:$7/2^+[633]$; $5/2^+$:$5/2^+[642]$.

(π): $7/2^-$:$7/2^-[523]$; $9/2^-$:$9/2^-[514]$; $7/2^+$:$7/2^+[404]$; $5/2^+$:$5/2^+[402]$; $1/2^+$:$1/2^+[411]$; $3/2^+$:$3/2^+[411]$.

$\Omega_j = 1/2$, as occurs in the present case where the $1/2^+[411]$ orbital is at the Fermi surface. In that circumstance and depending on the specific residual interactions, the $K_{\rm max} - 1$ state could be significantly lower in energy and closer to yrast. Examples are the 18^+ and 17^{+*} states from the same configuration (Table VI) where the latter is predicted to be nearly 800 keV lower and then the 19^- and 18^{-*} configurations in Table VII.

It should be noted that not all of the residual interactions required are available empirically, some are only estimates. Furthermore, the addition of the residual interactions deduced predominantly from two-quasiparticle cases can only be approximate for multiquasiparticle states, because the redistribution of particle and hole amplitudes is not taken into account in estimating the higher seniority cases. A more complete treatment would require the interaction to include explicitly the dependence on occupation probabilities, as given, for example, for two-quasiparticle cases by Massman *et al*. [40]. These would need to be generalized to the multiparticle case to use blocked wave functions, calculated self-consistently, for each configuration.

VII. DISCUSSION

A. Forbidden decay strengths

1. 6^+ Isomer

Substantiation of the 6^+ assignment to the 1518-keV isomer adds to the dilemma of understanding the transition strengths and decay pattern. The problem is that the branching *ratios* of the main decays in the 6^+ assignment cannot be explained on the basis of the Michailov, Michailovich generalizations of the Alaga rules as extended to *K*-forbidden transitions, a point discussed in the original article of Borggreen *et al*. [2]. Further, the 1265-keV E2 branch, which was not known at the time of the initial interpretation, but is now determined as a 2% branch, is very weak in absolute strength. The 1265 keV transition has partly been ignored in favor of consideration of the strength of the 992-keV transition, but the 1265-keV transition is retarded over the Weisskopf estimate by a factor of 1×10^{10}, which corresponds to a hindrance per degree of forbiddenness f_ν of ∼322, by far the largest value known in the region. To put this in context, the hindrances for the 6^+ configuration have been calculated [41] using a tunnelling prescription that has been successful in describing similar states in the hafnium and tungsten nuclei [42]. The predicted value [41] is $F = 7.5 \times 10^8$, which corresponds to $f_\nu = 93$. Although quantitative agreement is not obtained in all those cases and there are alternative treatments [43], the ^{174}Yb, 6^+ case represents essentially the only one in the model of Ref. [42], for which the experimental E2 hindrance is significantly *larger* (by a factor of 100) than the predicted value. The point here is that the tunnelling calculations should provide an upper limit, because the inclusion of other microscopic effects, such as configuration mixing, could be expected to enhance the

transition strength. The ^{174}Yb case, therefore, represents an unresolved problem requiring further attention.

B. 14^+ isomer; K mixing

In contrast to the decays from the 6^+ isomer, the E2 branch from the 14^+ state at 3699 keV has a reduced hindrance $f_\nu = 5.7$, and its other branches (M1 and E2) are also relatively fast. As discussed previously, the 14^+ state has two possible configurations, either a $\nu^2\pi^2$ configuration obtained by summing the 6^+ configuration and a $7/2^-[523] \otimes 9/2^-[514]$ π^2 configuration (Table VI) or, more likely the ν^4 alternative, which involves addition of the $7/2^+[633] \otimes 9/2^+[624]$ neutrons. The latter is supported by the observed alignment. This ν^4 configuration involves two $i_{13/2}$ neutrons and is the so-called t-band or Fermi-aligned configuration, the partner to the $K \sim 1$ aligned neutron configuration that is responsible for the backbending that occurs near $N = 104$–106 (see, for example, ^{179}W and ^{180}W [44,45]). This configuration will have an average projection of $K = 8$ for the component from the aligned neutrons, with a specific form of K mixing [29,30], although quantitative measures of the width of that K distribution for the ^{174}Yb case are not immediately available. From representative calculations (e.g. [46]) one can estimate typical distributions to have lower-K values with amplitudes of $\sim 0.62|K = 14\rangle + 0.48|K = 13\rangle + 0.26|K = 12\rangle + 0.10|K = 11\rangle \cdots$. The last component, for example, would give rise to an E2 transition that has forbiddenness $\nu = 3$ rather than 6. If the intrinsic forbiddenness is $f_\nu \sim 100$, this component would give an apparent value of $f_\nu \sim 14$, if it were interpreted as having $\nu = 6$.

A more general consideration, which may play an additional role, is that the 14^+ isomer is located in a region of high level density, well above the yrast line. Figure 9 shows E2 and E3 reduced hindrances for selected four-quasiparticle isomers, as originally given by Walker *et al.* [47], as a function of excitation with respect to a rigid rotor. The ^{174}Yb, 14^+ case in this formulation is $\sim$2.5 MeV above a nominal yrast line defined by rigid rotation [47]. The observed hindrance is consistent with the expected fall because of the random mixing with background states, as indicated by the solid curve [47]. Clearly, there are large fluctuations in the f_ν values. These would not be expected to be described by such a simple model, but the general trend seems to be reproduced. The points indicated by stars in this figure correspond to very fast decays from high-K states (mostly $K = 12^+$) directly to high-spin members of ground-state bands in even-even nuclei. These belong to another category of transitions that may arise not from admixtures in the primary isomer but from specific K mixing in the ground-state band in the region near and above the alignment of neutrons. (See Ref. [43] for schematic evaluations of some cases in terms of possible K mixing and shape-changes.)

C. Multiquasiparticle intrinsic states and systematics

A relatively large number of multiquasiparticle calculations have been carried out in the past decade with considerable success in describing multiquasiparticle yrast isomers in the Lu, Hf, and Ta nuclei. See, for example, Ref. [4,9,34,35,44].

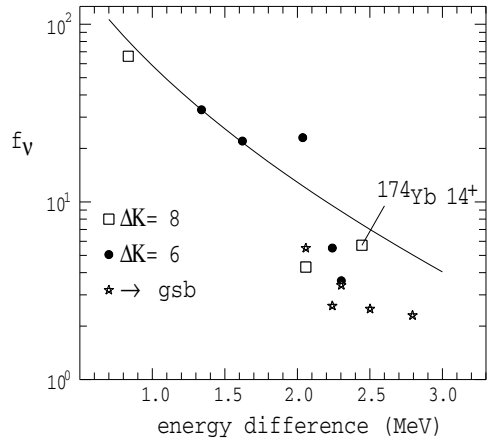

FIG. 9. Reduced hindrances for selected $\Delta K = 6$ and $\Delta K = 8$, E2 and E3 decays of four-quasiparticle states as a function of energy above a rigid rotor yrast line. The fast decay of the 14^+ isomer in ^{174}Yb is indicated. The solid curve represents the density-of-states estimate for $\Delta K = 6$ transitions given by Walker *et al.* [47].

The situation is not so clear cut in the present case because, as discussed, such multiquasiparticle states are less likely to be yrast, and the proton Fermi surface is near the low-Ω orbital, $1/2^+[411]$. One expectation of this different situation, which seems to be at least partly borne out in the assignments below, is that ν^4 configurations can compete with more "balanced" configurations, such as $\nu^2\pi^2$, for example, which are common at higher Z. (The lowest states usually involve approximately equal numbers of quasiprotons and quasineutrons.)

D. Comparison with multiquasiparticle calculations

As can be seen from Fig. 10 and Tables VI and VII there are a large number of intrinsic states expected at similar energies in the spin region 13–20$\hbar$. This situation is distinctly different from that in the Hf isotopes, where certain configurations, involving a few particular pairs of protons and neutrons, are significantly favored in energy, leading to high-K states that consistently occur low in the energy spectrum [48].

The relative separation of the ν^2, 6^+ and 7^- states is reproduced and the energies are only slightly underestimated. This could be because of a small underestimate in the pairing strength G_ν, but it should be noted that the 7^- state will have significant Coriolis mixing through the $7/2^+[633]$ component of its configuration with the family of $i_{13/2}$ orbitals. This will have the dual effect of lowering the energy of the lowest band (in this case the 7^- bandhead) while increasing the energy of the 8^- state from the related $9/2^+[624] \otimes 7/2^-[514]$ configuration. As stated, the situation in ^{174}Yb and ^{176}Yb is analogous to that in ^{180}Os and ^{182}Os, where a short-lived $K^\pi = 7^-$ isomer occurs in the former and a long-lived $K^\pi = 8^-$ isomer occurs in the latter.

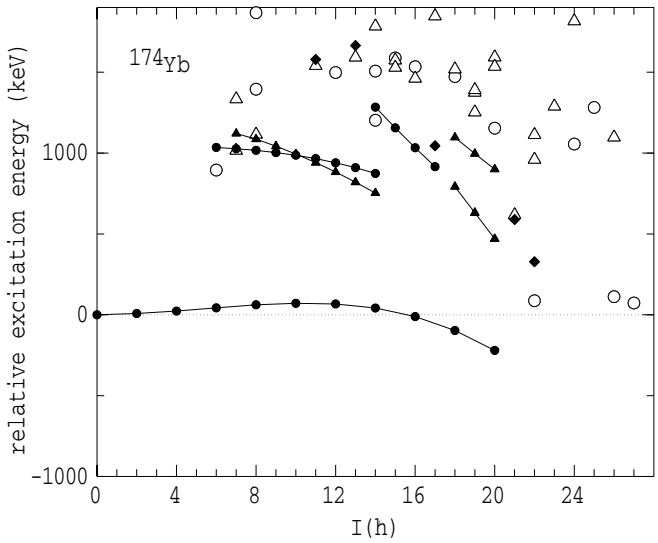

FIG. 10. Excitation energies of calculated and observed states expressed relative to a simple rotor with E(keV) $= 11.5 \times I(I+1)$. Open symbols represent the calculated intrinsic states (see Tables VI and VII), whereas filled symbols are experimental data. (Calculated states with $K \geqslant 23$ are of eight-quasiparticle character and are not included in the tables.) The lines connect rotational bands. Positive, negative, and unknown parities are given as circles, triangles, and diamonds, respectively.

In the high-spin regime, it can be seen that the $K = 21$ and $K = 22$ states at 5974 and 6147 keV are plausible candidates for $K^\pi = 21^-$ and 22^+ six-quasiparticle states predicted at 5930 and 5906 keV, respectively. Both involve the 14^+, ν^4 configuration coupled to the π^2 configurations; $7/2^-[523] \otimes 7/2^+[404]$ and $7/2^-[523] \otimes 9/2^-[514]$. The energy discrepancy (in terms of the predicted order rather than the absolute scale) is presumably because of the uncertainty in the position of the $7/2^+[404]$ orbital, which is not known experimentally in either ^{173}Tm or ^{175}Tm.

Also shown in Fig. 10 are the lowest eight-quasiparticle states predicted (all those with $K \geqslant 23$) with 24^+ and 25^+ states falling lowest. These spins are within the reach of the present reactions but as can be seen from the figure, the predicted states are significantly non-yrast and therefore likely to be only weakly populated.

From Fig. 10 and Tables VI and VII, it seems that there are no obvious low-lying states that should have been observed. The main difficulty in the comparison is in the region of spin 17–19, where there are no clear matches between the predicted and observed intrinsic states. For example, in the level scheme (Fig. 2) there are three levels that may be intrinsic states, at 4564 keV ((17^-)), 4725 keV ((18)), and 5030 keV ($(18^{(-)})$, 19), but the lowest 17^- state is predicted to be much higher at 5452 keV, the lowest 18^- state is the $K_{\max} - 1$ coupling predicted at 5366 keV (with the $K_{\max} = 19^-$ partner predicted at 5745 keV) and an 18^+ configuration is predicted at 5406 keV. It is possible that one or more of the observed states is a rotational member based on a lower lying intrinsic state, but again there are no obvious candidates for such band heads.

One possible explanation for this discrepancy is that the proton pairing strength is overestimated, but for several reasons, it is difficult to justify a significant decrease over the value used. More likely, the discrepancy is pointing to an overestimate of the $1/2^+[411] \otimes 9/2^-[514]$ two-proton energy and/or to an underestimate of the attractive residual interaction. This configuration is common to two of the predicted states, but it does not occur in any of the states that have been firmly assigned. As well, a number of the residual interactions involving the $1/2^+[411]$ orbital are estimates rather than empirical values. A similar problem was encountered in ^{177}Lu [9], where $K^\pi = 33/2^+$ and $K^\pi = 23/2^-$ isomers related by the same $1/2^+[411] \otimes 9/2^-[514]$ excitation are proposed, but although the $23/2^-$ state is reproduced by calculation, the energy of the $33/2^+$ state is overestimated by about 350 keV. As pointed out then [9], equivalent overestimates of the excitation energies are uncommon in higher-Z isotopes.

It is not proposed to make any further adjustment of the proton orbitals here, partly because of the experimental uncertainties but also because forthcoming results on ^{175}Yb and ^{176}Yb in conjunction with new results on the odd-A Lu isotopes should allow a more general evaluation of orbital positions (and possibly deformations) for the region. It should also be noted that in the systematic evaluations of Ref. [36] that included orbital-dependent deformations for odd-proton configurations, the relative energies of the $1/2^+[411]$, $7/2^+[404]$, and $3/2^+[411]$ states were in systematic disagreement with experiment.

VIII. SUMMARY

An extensive level scheme for the stable nucleus ^{174}Yb has been obtained from γ-ray spectroscopic studies with Gammasphere and "deep"-inelastic reactions induced by ^{136}Xe beams incident on targets of ^{174}Yb, ^{175}Lu, and ^{176}Lu. New results include the identification of the two-quasineutron $K^\pi = 7^-$ isomer and its associated rotational band, as well as the rotational band based on the known 6^+ isomer at 1518 keV. These band structures are linked through the decay of a $K^\pi = 14^+$, 80-ns isomer at 3699 keV that is assigned a four-quasineutron configuration. Other intrinsic states identified include $K = (21)$ and (22) states at 5974 and 6147 keV that have been assigned four-quasineutron/two-quasiproton configurations on the basis of comparisons with multiquasiparticle calculations. A number of uncertainties remain, both in the experimental assignments to the higher states and in the association with predicted configurations, some of which probably reflect the uncertainty in the position of proton orbitals in this region.

The ^{174}Yb nucleus exhibits a variety of K-forbidden transitions, ranging from the very hindered E2 transition from the 6^+ isomer that is yet to be explained satisfactorily to relatively fast transitions from the 14^+ isomer that can be attributed, in part, to specific Coriolis mixing in its configuration and to possible random mixing in the high-level density above the yrast line.

ACKNOWLEDGMENTS

We are indebted to R. B. Turkentine and J. Greene for producing the targets and to A. N. Wilson and P. M. Davidson who contributed to the ANU experiments. This work was supported by the ANSTO program for Access to Major Research Facilities, grant 02/03-H-05, the Australian Research Council Discovery projects DP0343027 and DP0345844, and the U.S. Department of Energy, Office of Nuclear Physics, under contract W-31-109-ENG-38 and Grant DE-FG02-94ER40848.

[1] E. Browne and Huo Junde, Nuclear Data Sheets **87**, 15 (1999).
[2] J. Borggreen, N. J. S. Hansen, J. Pederson, L. Westgaard, J. Zylic, and S. Bjornholm, Nucl. Phys. **A96**, 561 (1967).
[3] W. Gelletly, J. R. Larysz, H. G. Borner, R. F. Casten, W. F. Davidson, W. Mampe, K. Schreckenbach, and D. D. Warner, J. Phys. G **13**, 69 (1987).
[4] T. R. McGoram, G. D Dracoulis, T. Kibédi, A. P. Byrne, R. A. Bark, A. M. Baxter, and S. M. Mullins, Phys. Rev. C **62**, 031303(R) (2000).
[5] G. D. Dracoulis, C. Fahlander, and M. P. Fewell, Nucl. Phys. **A383**, 119 (1982).
[6] G. D. Dracoulis, unpublished data.
[7] C. Wheldon *et al*., Phys. Lett. **B425**, 239 (1998).
[8] T. R. McGoram, G. D. Dracoulis, T. Kibédi, A. P. Byrne, A. M. Baxter, and S. M. Mullins, to be published.
[9] G. D. Dracoulis *et al*., Phys. Lett. **B584**, 22 (2004).
[10] F. G. Kondev *et al*., Eur. Phys. J. A **22**, 23 (2004).
[11] R. Broda, M. A. Quader, P. J. Daly, R. V. F. Janssens, T. L. Khoo, W. C. Ma, and M. W. Drigert, Phys. Lett. **B251**, 245 (1990).
[12] R. Broda, C. T. Zhang, P. Kleinheinz, R. Menegazzo, K.-H Maier, H. Grawe, M. Schramm, R. Schubart, M. Lach, and S. Hofmann, Phys. Rev. C **49**, 575(R) (1995).
[13] J. F. C. Cocks *et al*., J. Phys. G, Nucl. Part. Phys. **26**, 23 (2000).
[14] R. V. F. Janssens and F. S. Stephens, Nucl. Phys. News **6**, 9 (1996).
[15] M. Cromaz, T. J. M. Symons, G. J. Lane, I. Y. Lee, and R. W. MacLeod, Nucl. Instrum. Meth. **462**, 519 (2001).
[16] L. P. Ekström and A. Nordlund, Nucl. Instrum. Methods Phys. Res. A **313**, 421 (1992).
[17] K. S. Krane and R. M. Steffen, Phys. Rev. C **2**, 724 (1970).
[18] Tables of F_k Coefficients and U_k Coefficients, in *Electro-Magnetic Interactions in Nuclear Spectroscopy*, edited by W. D. Hamilton (North Holland, Amsterdam, 1970), p. 890.
[19] L. P. Ekström, Comp. Phys. Commun. A **32**, 399 (1984).
[20] L. Gidefeldt, L. Erikson, Chr. Bargholtz, and L. Holmberg, Phys. Scripta **4**, 33 (1971).
[21] A. G. Schimdt, J. W. Mihelich, and E. G. Funk, Phys. Rev. C **9**, 2346 (1974).
[22] H. M. Youhana *et al*., Nucl. Phys. **A458**, 51 (1986).
[23] K. S. Krane, C. E. Olsen, S. S. Rosenblum, and W. A Steyert, Phys. Rev. C **12**, 1999 (1975).
[24] K. Neergård and P. Vogel, Nucl. Phys. **A145**, 33 (1970).
[25] K. T. Flanagan *et al*., Institute of Physics Conference on Nuclear Physics, Glasgow University, April 2003; to be published.
[26] T. Pawlat *et al*., Annual Report, Institute of Nuclear Physics, Krakow, Poland, 1998, p. 49; and references therein.
[27] R. Bengtsson, S. Frauendorf, and F.-R. May, At. Data Nucl. Data Tables **35**, 15 (1986).
[28] G. D. Dracoulis, F. G. Kondev, and P. M. Walker, Phys. Lett. **B419**, 7 (1998).
[29] S. Frauendorf, Nucl. Phys. **A557**, 259c (1993).
[30] S. Frauendorf, Phys. Scripta **24**, 349 (1981).
[31] S. Frauendorf, Nucl. Phys. **A677**, 115 (2000).
[32] S. M. Mullins *et al*., to be published; Nuclear Physics Department, Australian National University, Annual Report 1999 ANU-P/1420, p. 24.
[33] G. D. Dracoulis *et al*., to be published.
[34] Kirain Jain, O. Burglin, G. D. Dracoulis, B. Fabricius, N. Rowley, and P. M. Walker, Nucl. Phys. **A591**, 61 (1995).
[35] F. G. Kondev, G. D. Dracoulis, A. P. Byrne, T. Kibédi, and S. Bayer, Nucl. Phys. **A617**, 91 (1997).
[36] W. Nazarewicz, M. A. Riley, and J. D. Garrett, Nucl. Phys. **A512**, 61 (1990).
[37] P. Moller, J. R. Nix, W. D. Myers, and W. J. Swiatecki, At. Data Nucl. Data Tables **59**, 185 (1995).
[38] F. G. Kondev, G. D. Dracoulis, A. P. Byrne, and T. Kibédi, Nucl. Phys. **A632**, 473 (1998).
[39] F. G. Kondev, Ph.D. thesis, Australian National University 1996, unpublished.
[40] H. Massmann, J. O. Rasmussen, T. E. Ward, P. E. Haustein, and F. M. Bernthal, Phys. Rev. C **9**, 2312 (1974).
[41] Y. Shimizu. Private communication to G. D. Dracoulis, March 1996.
[42] K. Narimatsu, Y. R. Shimizu, and T. Shizuma, Nucl. Phys. **A601**, 69 (1996).
[43] B. Crowell *et al*., Phys. Rev. C **53**, 1173 (1996).
[44] P. M. Walker, G. D. Dracoulis, A. P. Byrne, B. Fabricius, T. Kibédi, A. E. Stuchbery, and N. Rowley, Nucl. Phys. **A568**, 397 (1994).
[45] P. M. Walker, K. C. Yeung, G. D. Dracoulis, P. H. Regan, G. J. Lane, P. M. Davidson, and A. E. Stuchbery, Phys. Lett. **B309**, 17 (1993).
[46] Makita Oi, Ahmad Ansari, Takatoshi Horibata, and Naoki Onishi, Phys. Lett. **B480**, 53 (2000).
[47] P. M. Walker *et al*., Phys. Lett. **B408**, 42 (1997).
[48] P. M. Walker and G. D. Dracoulis, Hyperfine Interactions **135**, 83 (2001).